**Atmospheric
Chemistry
and Physics
Discussions**

# Characterization of light-absorbing carbon particles at three altitudes in East Asian outflow by transmission electron microscopy

**J. Zhu, P. A. Crozier, and J. R. Anderson**

School for Engineering of Matter, Transport and Energy, Arizona State University, Tempe, Arizona, USA

Correspondence to: P. A. Crozier (crozier@asu.edu)

**ACPD**

12, 32945–32983, 2012

**Characterization of light-absorbing carbon particles**

J. Zhu et al.

Title Page

| Abstract | Introduction |
| Conclusions | References |
| Tables | Figures |

|◄ | ►|

◄ | ►

Back | Close

Full Screen / Esc

Printer-friendly Version

Interactive Discussion

## Abstract

The morphology, microstructure, and composition of the submicron fraction of individual light-absorbing carbon (LAC) particles collected by research aircraft during the ACE-Asia project above the Yellow Sea at altitudes of 120, 450 and 1500 m are investigated by transmission electron microscopy (TEM), and energy dispersive X-ray spectroscopy (EDS). Two types of carbonaceous particles, small spherule soot with graphitic spherules and amorphous carbonaceous spheres (brown carbon), are found at all altitudes in high concentration. For soot particles, emphasis of the study is on the component subparticles (spherules). The nanoscopic structures of the small spherule soot show no significant difference at three altitudes although the size distribution of primary spherules showed that 70 % of the total volume lies in the ranges 30–50, 50–85 and 30–50 nm, respectively. For the amorphous carbonaceous spheres, 70 % of the total volume from three altitudes lies in the range 200–350, 160–470 and 150–320 nm, respectively. Within the size fraction studied (submicron, with most particles in the range 50 to 500 nm) the number concentration ratios of the amorphous carbonaceous spheres to primary spherules in soot at altitudes of 120, 450 and 1500 m are about 1, 1.5 and 10, respectively and their volume ratios are about 260, 50 and 1400. Lower relative concentrations of large spherule soot with intermediate graphitic structure were observed at 120 m. Also, low relative number concentrations of carbon cenosphere were observed at 120 and 1500 m. A key result of the study is that in vertically stratified outflow from East Asia, the character of LAC may have strong variance with altitude thus resulting in optical characteristics that vary with altitude. Also, apparent "aging" of LAC deduced from samples at multiple ground stations may instead reflect differences in the original carbon aerosols.

# 1 Introduction

Light-absorbing carbon (LAC, inclusive of black carbon, brown carbon and humic-like substances) have a strong impact on the global climate by modifying the radiative forcing effects of greenhouse gases and other forcing agents. Some studies have surmised that LAC could be the second strongest contribution to current global warming by directly absorbing solar and terrestrial radiation (Ramanathan and Carmichael, 2008). Other radiative forcing effects, such as the "semi-direct" effect of aerosols on cloud cover (Hansen et al., 1997), can be important in the presence of significant LAC concentrations. In such a case, cloud cover is suppressed and the warming effect is enhanced. However, the vertical distribution of LAC can be complex and the position of LAC layers is important. Koch and Del Genio (2010) presented a review of an number of studies that consider the complexities that may arise from different vertical distributions of LAC and suggest that in some cases there may be a net negative semi-direct effect that can partially (or even perhaps entirely) offset the warming effect of direct absorption. Clearly both the vertical distribution and optical properties of LAC are important as to the net forcing. Spracklen et al. (2011) have discussed the possible role of LAC as cloud condensation nuclei (CNN) such that they also cool the climate by increasing cloud albedo. Whether this indirect forcing is regionally or globally important depends upon the extent to which LAC activate as CCN. Studies of important areas of marine stratiform clouds that have examined cloud droplet residues with electron microscopy have shown that LAC is not generally important as CCN because both size and composition are important (Twohy and Anderson, 2008) including in heavily polluted marine areas (Twohy et al., 2001; Hawkins et al., 2008). However, results of Stith et al. (2011) suggest that LAC from biomass burning may at times be important as ice nuclei for cirrus, although the LAC in this case is mostly internally mixed with other components so that the results are perhaps ambiguous. In any event, there are not enough data to evaluate any possible negative forcing due to LAC influence due to indirect effects on cloud albedo.

**Characterization of light-absorbing carbon particles**

J. Zhu et al.

Title Page

| Abstract | Introduction |
| Conclusions | References |
| Tables | Figures |

|◄ | ►|

◄ | ►

Back | Close

Full Screen / Esc

Printer-friendly Version

Interactive Discussion

The net radiative effect of LAC results from their multiple roles. Black carbon, of which soot is but one type, is estimated to contribute somewhere in the range of 10–50 % of the total tropospheric particulate matter (Zhang et al., 2008). After LAC are emitted to the atmosphere, they are subjected to aging processes such as absorption or condensation of gaseous species (Wyslouzil et al., 1994; Saathoff et al., 2003) and mixing with other aerosols, and oxidation (Liu et al., 2010; Lary et al., 1997; Rodriguez-Fortea et al., 2007). Processes, such as ice nucleation, cloud droplet formation (or scavenging) and gas degradation, would modify the structure and properties of the aerosols (Zhang et al., 2008).

There are numerous kinds of LAC with different morphology and structure. This diversity comes from variations in the combustion source, differences in combustion conditions and aging process undertaken in the atmosphere. The LAC from the combustion of different sources, such as biomass, coal, and gasoline have their own morphological, structural and compositional fingerprints. For example, LAC from biomass which usually carries minerals (Zhu et al., 2012c) contain potassium (Li et al., 2010). Variation in combustion conditions, such as the combustion temperature, pressure, and amount of oxygen, may also lead to different types of LAC. In addition, those LAC will be subjected to different aging processes once they enter the atmosphere. The combination of source combustion conditions and atmospheric aging processes undertaken can result in LAC with a variety of morphologies and properties. Black carbon is a strong absorber of light across a wide range of wavelengths of the solar spectrum. Brown carbon, a type of LAC attracting recent attention, has modest absorption in the visible spectral region and an enhanced absorption towards the near-UV spectral region (Alexander et al., 2008). Besides optical properties, the chemical properties of different aerosols can also vary. Soot shows good catalytic properties for transforming $NO_2$ into HONO in the presence of solar radiation (Monge et al., 2010).

Optical differences between LAC types arise from their different structures, size, morphology, aggregation state and compositions. The notable difference in soot and brown carbon is obviously related to their graphitic and amorphous structures. Even for

graphitic soot, microphysical processes, such as the ice nucleation on soot particles (Gorbunov et al., 2001), depends on the nanoscopic structure. Due the source effects, the local configuration of the graphene sheet in the soot varies significantly so it is necessary to describe these differences. A basic structural unit (BSU) has been developed (Chen et al., 2005) to characterize different graphene configurations. The BSU is described in terms of several indices which include the number of the stacking layers of graphene (layer No.), length of the stacking layers (La), thickness of the stacking layers (Lc) and the $d$-spacing of the stacking layers ($d_{0002}$).

On the other hand, morphology and aggregation of the particles will also lead to differences in physical properties. For example, additional interface modes in light absorption may arise when two or more particles are in contact with each other. Aggregates in different geometrical configurations may have significantly different absorption properties (Yin and Liu, 2010). Soot, is well-known to form agglomerates and fractal dimensions can be employed to describe the aggregation state (Olfert et al., 2007). The morphology affects the behavior of particles in the atmosphere and impacts human health.

In addition, it is necessary to understand the distribution and the structural differences in LAC with altitude. The aerosols at different altitudes may originate from different sources and have histories. In the case of stable stratification, local sources will contribute most strongly to the boundary layer. Of course if strong convective mixing has occurred then the vertical distribution of aerosols will be more complex. For the samples discussed here, vertical profiles of temperature and relative humidity indicated stable stratification. In such a case, aerosols in higher stable layers may be transported from significant distances. Arimoto et al. (2006) reported that the Asian dust collected below about 2 km altitude during ACE-Asia was commonly mixed with carbonaceous pollutants. However, there are limited studies on the size distribution of LAC, which could lead to uncertainty of the roles of the LAC such as the CCN (Pierce et al., 2007). It is important to analyze the relative concentrations of different types of LAC with altitude as the aerosols are typically treated in climate models as uniform

in optical properties at all altitudes. However, a detailed study about individual LAC particles including their structure and composition is difficult and has not been widely attempted. It is important to characterize the nanoscale structure of LAC recorded at different altitudes to develop a fundamental understand of their role in climate.

Transmission electron microscopy (TEM) is capable of providing local information on the structure, morphology and composition of LAC down to the nanoscale level (Chen et al., 2005). In our previous work, the optical properties of individual brown carbon aerosols collected above the Yellow Sea were studied in the TEM using monochromated electron energy-loss spectroscopy (Alexander et al., 2008). In the present work, the morphology, size, structure of the LAC collected from the same region are analyzed by TEM imaging and energy dispersive X-ray spectroscopy (EDS).

## 2 Experimental: sampling and characterization

The samples were collected during the spring 2001 Asian Pacific Regional Aerosol Characterization Experiment (ACE-Asia). The specimens analyzed here were sampled on 25 April 2001 during flight RF14 of the NCAR C-130 aircraft over the Yellow Sea at altitudes of 120, 450 and 1500 m within a stably stratified lower troposphere. The stratification was defined by parameters such as relative humidity and aerosol characteristics such as CCN concentrations and light scattering measured in real time during vertical profiles; it is possible that the various aerosol layers came from different source areas and had separate aging histories. The lowest altitude, 120 m, was within the marine boundary layer (MBL) as indicated by high RH (up to 76 %) and likely to be strongly influenced by local pollution including abundant ships and fishing boats observed from the NCAR C-130. Lower RH values (around 30 %) for the two higher layers indicate continental origin so the aerosols were not influenced by ship emissions. The sampled area was in dry continental air behind a cold front that moved from the northwest across the Yellow Sea region on the previous day. The samples containing brown

carbon described by Alexander et al. (2008) were obtained in more humid air in front of the same cold front on 23 April 2001 so were from completely different air masses.

A three-stage micro-impactor (California Measurements, Inc. Model MPS-3) was used to collect the samples. Supermicron particles were collected on stage 1 and are not discussed here. The nominal 50 % cut aerodynamic diameter range for stage 2 was 0.3 to 2 microns and for stage 3 0.05 to 0.3 microns. Because of the differences in morphology and density between standard spheres and the LAC particles collected, the cut sizes in practice could be quite different (the approximate upper cut size for stage 1 seemed to be about 0.5 microns). The results presented here are primarily from stage 3 and represent, based on SEM observations of single-stage filter samples for which absolute number concentration over the entire size range up to about 10 microns, the size fraction with by far the largest number concentration.

A 200 kV Schottky field emission analytical transmission electron microscope (JEOL JEM-2010F) equipped with thin window light element sensitive X-ray detector was used for the analysis of individual particles. Bright field imaging was used to detect the particle distribution, size, morphology, aggregation and mixing states. High resolution images were collected to study the microstructure of each particle. EDS was used to determine the elemental composition of individual particles with sensitivity for elements down to carbon. In order to maintain the initial status of the aerosol particle, and avoid radiation damage, low dose methods were adopted. During searching for and focusing on a sample area, the total electron dose was about $10^3$ electrons per nm$^2$. For collection of normal images, the electron dose was about $10^3$–$10^4$ electrons per nm$^2$. For high resolution images, the electron dose was about $10^6$ electrons per nm$^2$. Microscope alignment and focus adjustment were performed on areas of the sample adjacent to the particles of interest so that the particles were not irradiated. However, to get adequate signal-to-noise in the EDS, the electron beam was focused on the target particles. Acquisition times were typically 10 s to achieve adequate statistics in the spectra and the spectra were always collected after imaging.

**Characterization of light-absorbing carbon particles**

J. Zhu et al.

Full Screen / Esc

Printer-friendly Version

Interactive Discussion

The basic structural unit (BSU) of the soot spherules was measured from the high resolution TEM (HRTEM) images from 8 locations within spherules. The $d$-spacing of (0002) plane ($d_{0002}$), the stacked layer length (La), the number of the layers (Layer No.) of the BSU of the soot spherules were measured to compare the soot from the three altitudes. The fractal dimensions of the soot were calculated by a box-counting method. In this method, a square was defined that just enclosed the entire soot aggregate. Five concentric squares of decreasing size were then taken from this image. The number of the pixels ($N(s)$) ($s$ is the number of the pixels along the length of each square) occupied by soot spherules was obtained by using Photoshop image processing software. The fractal dimension is then given by the slope of $\log(N(s))$ against $\log(s)$ (Foroutan-pour et al., 1999).

## 3   Results and discussion

There are two main types of LAC found at all the three altitudes: graphitic soot and amorphous carbonaceous spheres similar to the brown carbon spheres described by Alexander et al. (2008). Their morphology, structure, composition and size distribution will be discussed in the following sections. Before giving a full description, three low magnification TEM images from three different altitudes are given in Fig. 1 to show an overview of the typical morphology and distribution of the aerosol on the TEM grids. The TEM grid used for 120 m altitude was a holey carbon film, while, for 450 and 1500 m, the grid was covered by a continuous carbon film. Many of the aerosol particles are spherical in shape. Some of the soot and amorphous carbonaceous spheres are marked by black and white arrows, respectively in Fig. 1. For altitude of 120 m, there is a high density of particles on the carbon support. In later sections, we will also show that most of the soot at altitude of 120 m is attached on other types of particles. The more spherically shaped large particles with size of about 100–300 nm are mostly amorphous carbonaceous spheres.

**Characterization of light-absorbing carbon particles**

J. Zhu et al.

Title Page

Abstract | Introduction

Conclusions | References

Tables | Figures

◄ | ►►

◄ | ►

Back | Close

Full Screen / Esc

Printer-friendly Version

Interactive Discussion

## 3.1 Soot

The TEM analysis shows that the soot from the three altitudes consists of primary small spherules in the size range 15–100 nm. Typical higher magnification TEM images of soot collected from altitudes of 120, 450 and 1500 m are shown in Figs. 2, 3, 4, respectively.

At 120 m altitude, the primary spherules of soot range from less than 20 to 70 nm. As shown in Fig. 2a, the soot spherules are aggregated together and have a turbostratic structure with multiple nuclei (Fig. 2b). The primary spherules, which can be discerned with separate boundaries from each other, are shown in Fig. 2a, b with dashed white lines. As shown in Table 1, the $d$-spacing of (0002) plane ($d_{0002}$) of the soot spherules is in the range of 0.37–0.46 nm, which is bigger than the $d_{0002}$ plane of graphite of 0.34 nm, even larger than 0.37–0.38 nm of soot particles prepared in research lab (Chen et al., 2005). The stacked layer length (La) of each BSU is about 1.04–2.39 nm and the number of the layers in each BSU is in 3–6. The EDS result (Fig. 2e) reveals that in addition to being mostly carbon, the soot had trace amounts of silicon, sulfur and potassium. No other element was detected other than copper, the signal for which comes from the TEM grid. It should be noted that small silicon peaks have been observed as a possible contaminant in similar samples from other projects in which we have participated, so some uncertainty exists in cases where silicon concentrations are this low.

The fractal dimension of the soot aggregate in Fig. 2a was calculated to be 1.48 by the box-counting method. However, it is important to point out that most of the soot spherules at this altitude are internally mixed with amorphous carbon. As shown in Fig. 2c, d, two soot spherules are attached to the surface of larger amorphous carbonaceous particles. A detailed characterization of this amorphous carbon will be discussed in later sections.

Figure 3 shows the TEM images of soot collected from the intermediate altitude, 450 m. The soot spherules range from 20 to 100 nm and can be grouped into two

categories, spherical (Fig. 3a, b), and non-spherical (Fig. 3c, d) subparticles. The individual soot particles are aggregates composed of either spherical or non-spherical subparticles, but not both. The spherical subparticles with onion-like structure have a size range of 40–100 nm, and contact each other by point to point contact. Soot par-
5   ticles composed of these spherical subparticles have fractal dimensions close to unity. The non-spherical subparticles with turbostratic structure and multiple nuclei, fused together, have diameter range of 20–40 nm, similar to those found at 120 m (Fig. 2a). The fractal dimension of the soot particles composed of non-spherical subparticles is 1.13. For the microstructure of those two kinds of soot spherules (Table 1), the layer
10  number ranges of the spherical and non-spherical particles are 2–4 and 3–4, respectively. Their La values are 0.67–1.27 and 0.72–1.49 nm, respectively. Their $d$-spacing are about 0.41–0.53 and 0.34–0.45 nm, respectively. Typical EDS (Fig. 3e, f) collected from the two kinds of soot indicate that the spherical soot contains less silicon and oxygen than that of non-spherical ones.

15      The differences in morphologies and aggregation of the spherical and non-spherical subparticles may arise from different source conditions and/or atmospheric aging processes although it is perhaps difficult to imagine how aging would alter the fundamental internal structure of a spherule. Atmospheric aging process can apparently change the fractal dimension of soot particles made of aggregates of spherules (Carabali et al.,
20  2012) but there is no clear evidence with regard to the subparticles. The difference concerning point of contact or fusing between the subparticles is most likely to be associated with different combustion conditions at the sources. It was reported that soot with a high content of unburned hydrocarbons would fuse together (Widmann et al., 2003; Leonard et al., 1994). More work on LAC from different sources in East Asia is
25  needed to make any conclusions about origins of the different types discussed here.

    For the 1500 m sample, soot with primary spherules of 30–40 nm is found on the carbon film substrate (Fig. 4a, b). Mixed states of soot with amorphous carbonaceous spheres are also found (Fig. 4c), similar to the altitude of 120 m (Fig. 2c). The soot has a turbostratic structure with BSU similar to those from other two altitudes. The mixed

Title Page

Abstract | Introduction

Conclusions | References

Tables | Figures

|◄ | ►|

◄ | ►

Back | Close

Full Screen / Esc

Printer-friendly Version

Interactive Discussion

status for the particles collected at 1500 m is reasonable because the longer aging time in the atmosphere increases the probability of collisions and interactions between particles. The EDS (Fig. 4d) result shows the soot have traces of silicon, oxygen, and sulfur. The fractal dimension of the soot in Fig. 4a is measured to be 1.36.

From the EDS results of the soot at the three altitudes, all of them contain mainly carbon. However, some soot at 120 m may contain oxygen, sulfur, silicon and/or potassium. Some of soot at 450 m contains oxygen and silicon, whereas the soot at 1500 m contains oxygen and sulfur. The potassium suggests some of the soot at 120 m is from the biomass burning. The soot from the other two altitudes possibly comes from combustion of fossil fuels.

The size distributions and relative number concentrations of primary spherules in soot were determined from a 160 $\mu m^2$ area on two low magnification images recorded at two different locations on the grids. The primary spherules in soot attached on other kinds of aerosol particles are also included in the analysis. Figure 5a shows the size distribution of the primary spherules of the soot. Clearly the soot primary spherules at different altitudes have different size distributions. For altitude of 120, 450 and 1500 m, their size range is 15 to 70, 20 to 100 and 20 to 60 nm, respectively. The weighted average sizes by number for the primary spherules of the soot are 30, 55 and 35 nm for altitudes of 120, 450 and 1500 m, respectively. For altitudes of 120 and 1500 m, 70 % of the soot subparticles lies in the range of 20–40 nm with a unimodal distribution. However, the soot subparticles from 450 m have a much broader distribution with 70 % of the subparticles lying in the range 30–80 nm. The spherules from 450 m have a bimodal distribution with peaks at around 35 and 65, respectively.

While it would be useful to know the relative mass concentrations of the different LAC particle types, the densities of the soot and amorphous carbonaceous sphere are unknown and so we have characterized the relative volume concentrations. Figure 5b shows the volume distribution with size of the soot spherules at three altitudes. The weighted average sizes by volume for the primary spherules of the soot are 40, 70 and 40 nm for altitudes of 120, 450 and 1500 m, respectively. Spherules in 30–50 nm size

Title Page

Abstract | Introduction

Conclusions | References

Tables | Figures

◄ | ►|

◄ | ►

Back | Close

Full Screen / Esc

Printer-friendly Version

Interactive Discussion

range contribute more than 70 % of their total volume at altitude of 120 m. The range changes into 50–85 nm at altitude of 450 m. For altitude of 1500 m, the soot in range of 30–50 nm holds more than about 70 % of the total relative volume.

Careful characterization of the primary particle size in the soot aggregates may help in identifying the possible origin of the soot particles (although the existing body of such work is far from exhaustive when considering the diversity of combustion sources in a region like East Asia). The primary soot spherules are formed from pyrolysis of volatile organic compounds during combustion. Nuclei first form by condensation during cooling and then grow by additional condensation and then multiple nuclei form aggregates through the coalescence of subparticles. Catalysts are not necessary for the formation of graphitic soot, different from other types of graphitic carbon, like carbon nanotubes (Zhu et al., 2012a,b). Griffin reported that the morphology of the soot is strongly related to their origin (Griffin and Goldberg, 1979). For instance, spherules from certain diesel engines are within a narrow range around 25 nm with a variation range of 33–36 % in different operation conditions (Lapuerta et al., 2007). However, a larger range of combustion conditions that might be possible has not been addressed yet, even for a single source type such as diesel.

Our results are also consistent with the soot collected from other regions with slight differences. Fu et al. (2008) reported that the spherules from the fuel oil burning at a small city of Tokaimura near the highway were spherical and 50 nm in size. Coz and Leck (2011) reported freshly formed soot aggregates in Southern Asia had an open branched structure, however, after long-range transport, the soot aggregates became compact with a complex internal mixture, and eventually coated with layer consisted with organic and inorganic compounds. However, when considering LAC measured at different ground stations when Lagrangian advection conditions cannot be shown, the conclusion of aging may be subject to uncertainty. Most of the reported work focused on the soot with spherules in size range of 20–60 nm. Our finding indicates that typical small spherule soot can have a much broader subparticle size range up to 100 nm. And

**Characterization of light-absorbing carbon particles**

J. Zhu et al.

at certain altitudes, i.e. 450 m, the subparticles in 50–90 nm size range dominate the whole volume of soot.

## 3.2 Amorphous carbonaceous spheres

Consistent with our previous report (Alexander et al., 2008) on aerosols from a different ACE-Asia flight (RF13 on 23 April 2001 and on the opposite side of a frontal passage from RF14), another significant kind of LAC found at the three altitudes are carbonaceous spheres. The carbonaceous spheres, larger than the soot spherules, are amorphous, and predominantly isolated. As such, they are morphologically similar to the "tar balls" described by Posfai et al. (2004), although the absence of potassium in the carbonaceous spheres in East Asian outflow described here suggests that they may not have the same biomass-burning origin as "tar balls". Morphologically similar spheres have been observed in a variety of settings (e.g. the Phoenix, Arizona urban aerosol as shown by SEM images by Anderson et al., 2006 where biomass burning is an insignificant source), so there may be a variety of such individual carbon spheres. Higher magnification TEM images from these LAC particles for altitudes of 120, 450 and 1500 m are shown in Figs. 6, 7, 8, respectively.

At 120 m altitude, most of the spheres are found mixed with other kinds of aerosol particles. Figure 6a is an amorphous brown carbon sphere mixed with other irregular carbon particles. The dielectric and optical properties of the brown carbon will be discussed in a future paper. Two soot spherules (indicated by arrows) are also found on the surface of the brown carbon. Figure 6b is an amorphous carbonaceous sphere touching some shell-like residue which resulted after electron beam irradiation of the orginal material that may have been organic. To get volume information from the TEM images, we investigated the 3-D particle shape by examining intensity line profiles across the TEM image of particles as shown in Fig. 6d. To a first approximation, the average image intensity from thin amorphous carbon varies linearly with mass thickness. The elliptical profile I of Fig. 6d is consistent with a a solid 3-D spherical particle. Another sphere is shown in Fig. 6c on top of the TEM carbon film with part suspended

over the vacuum. Two line profiles are collected across the sphere. All the three line profiles have different lengths. The profiles are scaled to the same width in Fig. 6 to make it easier to compare their shapes. The profile from the part of the particle suspended over the vacuum is in the form of a smooth elliptical curve which would be expected from a spherical shaped particle (profile II). However, the other profile from the area of the particle lying partially on the carbon film (profile III) shows discontinuities in the slope at the two ends of the profile (see the arrows) and a relatively constant intensity in the middle. At first glance, a flat profile suggest that the particle may be flattened perhaps as a result of colliding with the carbon film during the sample collecting process. However, further analysis discussed below reveals that this interpretation is not correct and that the particles are indeed spherical in shape.

For samples from altitudes of 450 and 1500 m, most of the amorphous brown carbon spheres on the TEM grids are also found to have the nearly flattened line profile as seen in Fig. 7. In some cases these spheres were found to have tails as shown in Fig. 7b. In contrast to observations at 120 m, the amorphous carbonaceous spheres at 450 m consisted mostly of isolated particles dispersed on the surface of the carbon film without internal mixing with other aerosol types.

A typical brown carbon particle collected at 1500 m is shown in Fig. 8a. It is amorphous and its line profile, similar to that in Fig. 7, has a nearly flattened profile. A coating-like contrast is found on its surface. The sample was tilted over a range of angles and images recorded to obtain more information about the nature of the coating. As shown in Fig. 8a, b, c, the width of the arrowed edge changed with tilt, which indicated the coating is not continuous over the surface of the particle. The chemical composition of the coating has no detectable difference from the spheres according to EDS. The coating surrounding the spheres is postulated to be a viscous organic layer. Spheres with a tail in the form of a viscous structure were also found. This kind of structure has the same composition as the sphere without tails (Fig. 8d). Both of them contain mainly carbon, oxygen and trace sulfur (Fig. 8f–I). However, the tail also contains a high concentration of potassium (Fig. 8f–II) and could be formed from organic

hydrocarbon mixed with a potassium salt. The lack of circular symmetry in these structures implies that this potassium containing organic species was not orginally completely coating the sphere but may have been in the form of a small particle attached to the side of the sphere. Most spheres are isolated on the carbon film, however, a small fraction of them are connected together (Fig. 8e). Because of the radial distribution of impacted particles on the grids, in places with the high particle loading there may be apparent aggregation on the TEM grid whereas the particles were in fact separated in the atmosphere (however, the particle in Fig. 8e is likely to be as it was before sampling). The actual degree of aggregation is best assessed where the loading is light.

EDS spectra of the amorphous spheres at the three altitudes are similar to each other. All contained carbon, oxygen, and minor sulfur and silicon. The amorphous carbonaceous spheres might be from the same type of source, although this is still uncertain. The absence of potassium in the spheres suggests that, unlike the tarballs from the work of Posfai et al. (2004), they are not generated by biomass combustion.

In order to check the relationship between particle morphology and the image intensity profiles, Beer's absorption law, $I_t = I_0 e^{(-\alpha t)}$, was used investigate the intensity variation with particle thickness for the imaging conditions employed. This was necessary to rule out significant shape deformation when the particles impacted the carbon support film and validate our assumption that the particles were essentially spherical in shape. First, the absorption coefficient ($\alpha$) was calculated from the amorphous carbonaceous spheres (one example is in Fig. 6b) suspended in vacuum on a holey carbon grid (120 m sample). The spheres overhanging the holes should not show significant deformation and can be used to determine the parameter $\alpha$. The intensity $I_t$ and $I_0$ are the intensity integrals of an area of $20 \times 20$ pixels in the center of the spheres and from the background (vacuum or the carbon film) in TEM images, respectively. As shown in Fig. 9a, $\alpha$ equals the slope of the $\ln(I_0/I_t)$ versus $t$ curve and is linear relationship over a wide size range (here $t$ is the measured diameter of the carbonaceous spheres). The value of $\alpha$ is found to be $0.0023\,\text{nm}^{-1}$ under our TEM imaging conditions. The $\alpha$ value will vary with different collection angles (Zhang et al.,

**Characterization of light-absorbing carbon particles**

J. Zhu et al.

2012). It should be pointed out that the data in Fig. 9a are from tens of particles on two holey carbon grids. All the points lie along a straight line suggesting that the method of determining the absorption coefficient ($\alpha$) is reasonable. We now assume that the amorphous carbonaceous particles on a continuous carbon film grid from the other two altitudes have similar electron scattering strengths and we use the same absorption coefficient $\alpha$ to determine their thickness in the electron beam direction. The calculated thickness versus the measured diameter of the particles is shown in Fig. 9b. The slope was about 0.96 revealing the thickness is comparable to the measured diameter. So we can conclude that these particles also have a spherical shape and there was negligible plastic deformation during the collision with carbon film. We also simulated the intensity line profile across a spherical sphere on a carbon film using the absorption coefficient ($\alpha$). The simulated line profiles (not shown) matched the experimental ones further validating this model.

The number and volume distributions of amorphous carbonaceous spheres (Fig. 10) were determined from a 160 µm$^2$ area (the same area used to analyze the soot) on two low magnification images recorded at two different locations on the grids. The volume calculation depends on the confirmation of the 3-D shape of the particles. The weighted average diameters by number (and by volume) are 200, 170 and 160 nm (290, 280, and 235 nm), for altitudes of 120, 450 and 1500 m, respectively. The brown carbon spheres at 120 m range from 50 to 350 nm with 70 % in 125–275 nm. About 1 % of the spheres are in the range of 525–550 nm. For 450 m altitude, the spheres have a large size range spanning 50 to 475 nm with about 70 % lying in 100–225 nm. For 1500 m, the spheres range from 50–350 nm with about 70 % in 100–225 nm. Figure 10b shows the volume distribution with the distribution also varying with altitude. At 120 m, spheres in 200–350 nm contribute about 70 % of the total volume. The small quantity of large spheres above 500 nm takes about 18 % of the total volume. At 450 m, 70 % of the total volume lay in a wide range of 160–470 nm. In contrast, the relative smaller spheres in 150–325 nm takes about 70 % of the total volume for altitude of 1500 m.

Title Page

| Abstract | Introduction |
| Conclusions | References |
| Tables | Figures |

|◄ | ►|

| ◄ | ► |

| Back | Close |

Full Screen / Esc

Printer-friendly Version

Interactive Discussion

## 3.3 Minor types of LAC particles

In addition to the soot with primary spherule size in the range of 20–100 nm (which we term small spherule soot) shown in Sect. 3.1, lower concentrations of a soot type made of larger graphitic spherules (Fig. 11) were also found in samples collected at 120 m. This kind of soot has a primary spherule size in the range of 130–230 nm (Fig. 11a). They are termed large spherule soot to differentiate them from the small spherule soot previously described. The large spherule soot is graphitic as shown in the HRTEM image in Fig. 11b and spherules are connected together to give a cylinder-like structure. The volume of large spherule soot is about $29 \times 10^6$ nm$^3$ in area of 6400 µm$^2$. Their volume ratio to the small soot in the same area is about 0.11, comprising about 10 percent of the soot by volume. So, it is necessary to take into account this kind of large spherule soot even though in lower concentration. Onion-like small soot spherules with diameter about 40 nm were occasionally attached on the surface of the large spherule soot (Fig. 11b). No large spherule soot was found at 450 and 1500 m altitude in this case; this perhaps suggests a marine or coastal origin such as ship emissions or coal-fired power plants that are present along the coast of the Yellow Sea. The air mass sampled at 120 was in the MBL whereas the higher altitudes were in dry continental air. Chen et al. (2005) found similar large spherule soot with primary spherule size about 100–400 nm in bituminous-coal-derived sample, but not in samples from diesel or residual oil combustion. Large spherule soot with similar size and morphology has also been observed in the Phoenix, Arizona aerosol (Anderson et al., 2006) where neither ships nor coal combustion are likely sources. Again, without characterizing the many diverse combustion sources in the region the origin of the various carbonaceous particle types remains uncertain.

Another minor type of LAC is carbon cenopheres, hollow spheres which were also found in another ACE-Asia C-130 flight, RF13 on 23 April 2001 (Clarke et al., 2004) and on ACE-Asia samples collected by research ship (Quinn et al., 2004). On stages 2 and 3 they were observed only at altitudes of 120 and 1500 m. TEM images and their EDS

Title Page

Abstract | Introduction

Conclusions | References

Tables | Figures

◄ | ►

◄ | ►

Back | Close

Full Screen / Esc

Printer-friendly Version

Interactive Discussion

of the cenospheres from altitude of 120 m are shown in Fig. 12. From the HRTEM image (Fig. 12c), the cenospheres are amorphous rather than graphitic (Quinn et al., 2004; Clarke et al., 2004). From the contrast of the images, there is a empty space inside the carbon spheres in Fig. 12a, b (as expected). The hollow spheres found at 1500 m have similar structure and composition with those at 120 m with diameters in the range of 150–250 nm. The ratio of the inner diameter to outer diameter was relatively constant at around 0.6–0.65, suggesting that these cenospheres may originate from similar combustion conditions. The cenospheres are a common product of pyrolysis during inefficient combustion of heavy fuel oil (Bertran and Marques, 2004). During the heating of the fuel oil droplet, the gas from the evaporation of lighter compounds surrounds the droplet and burns, which reduces the contact of oxygen molecules with the oil droplet. Then, the surface of the droplet will pyrolyze quickly and form a solid state carbon as the cenosphere shell. They are very stable under the high electron beam current used in TEM analysis. EDS of the cenospheres indicates they contain high amounts of sulfur besides carbon and traces of silicon. The sulfur residues from the $SO_2$ gas which is probably responsible for the formation of the hole. Xie et al. (2007) found same kind of LAC collected in the marine boundary layer, with spherical shape, porous structure and high sulfur content from residual oil combustion by ship emissions. So the cenospheres may also come from the residual oil combustion. The number of cenospheres is about 5 on area of 160 $\mu$m$^2$. If we assume the holes inside the particles are spherical, their total volume can be calculated to be about $12 \times 10^6$ nm$^3$. Within the same sampling area, the total number of amorphous carbonaceous spheres was 327 with corresponding total volume of about $18 \times 10^8$ nm$^3$ (Table 2). Thus the cenospheres are less than 1 % in the total volume and would be negligible for the light absorption in the submicron range of stages 2 and 3. However, much larger cenospheres (up to at least 10 $\mu$m diameter) are observed by SEM in corresponding single-stage filter samples.

## 3.4 Summary of the statistics of soot and amorphous carbonaceous spheres

For the size fraction studied by TEM, the total number and volume of primary spherules in soot and separate brown carbon spheres analyzed in the same grid areas are listed in Table 2 in order to evaluate the relative importance of the two major carbonaceous particle types. The absolute numbers are not significant because of the method of sampling. In all cases, the volume of brown carbon is greater than the volume of soot (as determined by measuring individual spherules), with the most extreme case at 1500 m. The number of soot spherules (but not soot particles, which are comprised of multiple spherules) is similar to the number of brown carbon spheres at 120 m, but only a tenth of the number of brown carbon particles at 1500 m. The number ratio of brown carbon to actual soot particles is even greater. The larger diameters of brown carbon spheres compared to soot spherule diameters combined with the number ratios make brown carbon the dominant carbonaceous particle type in the submicron range for the air masses sampled. Also, the aerosol layers sampled at different altitudes are clearly different with regard to the carbonaceous particle population.

## 4 Conclusions

During a research flight above the Yellow Sea on 25 April 2001, several kinds of LAC were observed at sampled altitudes of 120, 450 and 1500 m in a stratified lower troposphere during an outbreak of East Asian dust and pollution. The LAC included high number concentrations of small spherule soot and amorphous carbonaceous spheres (brown carbon) along with lower relative concentrations of large spherule soot and carbon cenospheres in the submicron fraction. The soot at all three altitudes was graphitic, with similar basic structural units but fractal dimensions that were slightly different. At 120 m, the small spherule soot contained mainly carbon as well as oxygen, sulfur, and a small amount of silicon and/or potassium. Soot consisting of non-spherical primary particles at 450 m contained oxygen and perhaps silicon, whereas the soot at

Title Page

Abstract | Introduction

Conclusions | References

Tables | Figures

◄ | ►

◄ | ►

Back | Close

Full Screen / Esc

Printer-friendly Version

Interactive Discussion

1500 m contained oxygen and sulfur. The small spherule soot was often mixed with other aerosol particles at the low altitude within the MBL. The amorphous carbonaceous spheres all had a similar chemical composition with carbon, oxygen, and minor sulfur and perhaps silicon present in samples from the three altitudes. Image intensity analysis confirmed their spherical shape and some particles had a surface coating of a separate but undetermined carbon-bearing phase.

The relative number concentration of soot spherules was comparable to that of brown carbon spheres at altitudes of 120 and 450 m. However, the numbers of carbonaceous spheres were ten times that of the soot spherules at 1500 m. For the primary spherules of small spherule soot, 70 % of the total volume lay in size range 30–50, 50–85 and 30–50 nm, respectively, for the ascending altitudes. For the brown carbon spheres, 70 % of the total volume from lay in the size range 200–350, 160–470 and 150–320 nm at 120, 450 and 1500 m, respectively. The relative volume of the carbonaceous spheres was about 260, 50 and 1400 times that of the small spherule soot at 120, 450 and 1500 m, respectively. Lower number concentrations of large spherule soot with a graphitic structure contributed about 10 % of the soot volume. The amorphous hollow carbon cenospheres were less than 1 % of volume of the amorphous carbonaceous spheres.

The general conclusion to be drawn from this work is that in a stably stratified troposphere, such as was commonly encountered for East Asian outflow in ACE-Asia, the vertical distribution of LAC types is not homogeneous and therefore the radiative effects of LAC are more complex than if the distribution was more uniform. The presence of an overwhelming majority of LAC present in the form of amorphous brown carbon spheres in outflow above the Yellow Sea in these samples is striking and shows the need for understanding more than just bulk elemental carbon and organic carbon fractions of East Asian aerosols. Another conclusion to be drawn from the vertical variation in aerosol is that sampling from only ground stations is inadequate for determining the radiation forcing effects of pollutant outflow containing light absorbing carbon. It is important to be cautious concerning conclusions about LAC aging based on sampling

involving non-Lagrangian advection of what may be different aerosols in a vertically inhomogeneous lower troposphere.

# References

Alexander, D. T., Crozier, P. A., and Anderson, J. R.: Brown carbon spheres in East Asian outflow and their optical properties, Science, 321, 833–836, doi:10.1126/science.1155296, 2008.

Anderson, J. R., Moor, G., Femando, H., and Hyde, P.: A field study of particulate emissions from major roadways in the Phoenix Airshed, Arizona Dept. of Transportation, Phoenix, ATRC Report 495, 101, 2006.

Arimoto, R., Kim, Y. J., Kim, Y. P., Quinn, P. K., Bates, T. S., Anderson, T. L., Gong, S., Uno, I., Chin, M., Huebert, B. J., Clarke, A. D., Shinozuka, Y., Weber, R. J., Anderson, J. R., Guazzotti, S. A., Sullivan, R. C., Sodeman, D. A., Prather, K. A., and Sokolik, I. N.: Characterization of Asian dust during ACE-Asia, Global Planet. Change, 52, 23–56, doi:10.1016/j.gloplacha.2006.02.013, 2006.

Bertran, C. A. and Marques, C. S. T.: Study of the particulate matter emitted from residual oil combustion and natural gas reburning, J. Brazil. Chem. Soc., 15, 548–555, doi:10.1590/s0103-50532004000400017, 2004.

Carabali, G., Mamani-Paco, R., Castro, T., Peralta, O., Herrera, E., and Trujillo, B.: Optical properties, morphology and elemental composition of atmospheric particles at T1 supersite on MILAGRO campaign, Atmos. Chem. Phys., 12, 2747–2755, doi:10.5194/acp-12-2747-2012, 2012.

Chen, Y. Z., Shah, N., Braun, A., Huggins, F. E., and Huffman, G. P.: Electron microscopy investigation of carbonaceous particulate matter generated by combustion of fossil fuels, Energ. Fuel., 19, 1644–1651, doi:10.1021/ef049736y, 2005.

**Characterization of light-absorbing carbon particles**

J. Zhu et al.

Title Page

| Abstract | Introduction |
| Conclusions | References |
| Tables | Figures |

|◄ | ►|

◄ | ►

Back | Close

Full Screen / Esc

Printer-friendly Version

Interactive Discussion

Clarke, A. D., Shinozuka, Y., Kapustin, V. N., Howell, S., Huebert, B., Doherty, S., Anderson, T., Covert, D., Anderson, J., Hua, X., Moore, K. G., McNaughton, C., Carmichael, G., and Weber, R.: Size distributions and mixtures of dust and black carbon aerosol in Asian outflow: physiochemistry and optical properties, J. Geophys. Res.-Atmos., 109, D15S09, doi:10.1029/2003jd004378, 2004.

Coz, E. and Leck, C.: Morphology and state of mixture of atmospheric soot aggregates during the winter season over Southern Asia – a quantitative approach, Tellus B, 63, 107–116, doi:10.1111/j.1600-0889.2010.00513.x, 2011.

Foroutan-pour, K., Dutilleul, P., and Smith, D. L.: Advances in the implementation of the box-counting method of fractal dimension estimation, Appl. Math. Comput., 105, 195–210, doi:10.1016/s0096-3003(98)10096-6, 1999.

Fu, F. F., Watanabe, K., Shinohara, N., Xu, X. Q., Xu, L. J., and Akagi, T.: Morphological and light-absorption characteristics of individual BC particles collected in an urban seaside area at Tokaimura, eastern central Japan, Sci. Total Environ., 393, 273–282, doi:10.1016/j.scitotenv.2008.01.018, 2008.

Gorbunov, B., Baklanov, A., Kakutkina, N., Windsor, H. L., and Toumi, R.: Ice nucleation on soot particles, J. Aerosol. Sci., 32, 199–215, doi:10.1016/s0021-8502(00)00077-x, 2001.

Griffin, J. J. and Goldberg, E. D.: Morphologies and origin of elemental carbon in the environment, Science, 206, 563–565, doi:10.1126/science.206.4418.563, 1979.

Hansen, J., Sato, M., and Ruedy, R.: Radiative forcing and climate response, J. Geophys. Res.-Atmos., 102, 6831–6864, doi:10.1029/96jd03436, 1997.

Hawkins, L. N., Russell, L. M., Twohy, C. H., and Anderson, J. R.: Uniform particle-droplet partitioning of 18 organic and elemental components measured in and below DYCOMS-II stratocumulus clouds, J. Geophys. Res.-Atmos., 113, D15S09, doi:10.1029/2007jd009150, 2008.

Koch, D. and Del Genio, A. D.: Black carbon semi-direct effects on cloud cover: review and synthesis, Atmos. Chem. Phys., 10, 7685–7696, doi:10.5194/acp-10-7685-2010, 2010.

Lapuerta, M., Martos, F. J., and Herreros, J. M.: Effect of engine operating conditions on the size of primary particles composing diesel soot agglomerates, J. Aerosol. Sci., 38, 455–466, doi:10.1016/j.jaerosci.2007.02.001, 2007.

Lary, D. J., Lee, A. M., Toumi, R., Newchurch, M. J., Pirre, M., and Renard, J. B.: Carbon aerosols and atmospheric photochemistry, J. Geophys. Res.-Atmos., 102, 3671–3682, doi:10.1029/96jd02969, 1997.

**Characterization of light-absorbing carbon particles**

J. Zhu et al.

Leonard, S., Mulholland, G. W., Puri, R., and Santoro, R. J.: Generation of CO and smoke during underventilated combustion, Combust. Flame, 98, 20–34, doi:10.1016/0010-2180(94)90195-3, 1994.

Li, W. J., Shao, L. Y., and Buseck, P. R.: Haze types in Beijing and the influence of agricultural biomass burning, Atmos. Chem. Phys., 10, 8119–8130, doi:10.5194/acp-10-8119-2010, 2010.

Liu, Y. C., Liu, C., Ma, J. Z., Ma, Q. X., and He, H.: Structural and hygroscopic changes of soot during heterogeneous reaction with O-3, Phys. Chem. Chem. Phys., 12, 10896–10903, doi:10.1039/c0cp00402b, 2010.

Monge, M. E., D'Anna, B., Mazri, L., Giroir-Fendler, A., Ammann, M., Donaldson, D. J., and George, C.: Light changes the atmospheric reactivity of soot, P. Natl. Acad. Sci. USA, 107, 6605–6609, doi:10.1073/pnas.0908341107, 2010.

Olfert, J. S., Symonds, J. P. R., and Collings, N.: The effective density and fractal dimension of particles emitted from a light-duty diesel vehicle with a diesel oxidation catalyst, J. Aerosol. Sci., 38, 69–82, doi:10.1016/j.jaerosci.2006.10.002, 2007.

Pierce, J. R., Chen, K., and Adams, P. J.: Contribution of primary carbonaceous aerosol to cloud condensation nuclei: processes and uncertainties evaluated with a global aerosol microphysics model, Atmos. Chem. Phys., 7, 5447–5466, doi:10.5194/acp-7-5447-2007, 2007.

Quinn, P. K., Coffman, D. J., Bates, T. S., Welton, E. J., Covert, D. S., Miller, T. L., Johnson, J. E., Maria, S., Russell, L., Arimoto, R., Carrico, C. M., Rood, M. J., and Anderson, J.: Aerosol optical properties measured on board the *Ronald H*, brown during ACE-Asia as a function of aerosol chemical composition and source region, J. Geophys. Res.-Atmos., 109, D19s01, doi:10.1029/2003jd004010, 2004.

Ramanathan, V. and Carmichael, G.: Global and regional climate changes due to black carbon, Nat. Geosci., 1, 221–227, doi:10.1038/ngeo156, 2008.

Rodriguez-Fortea, A., Iannuzzi, M., and Parrinello, M.: Ab initio molecular dynamics study of heterogeneous nitric acid decomposition reactions on graphite surfaces, J. Phys. Chem. C, 111, 2251–2258, doi:10.1021/jp066581h, 2007.

Saathoff, H., Naumann, K. H., Schnaiter, M., Schock, W., Mohler, O., Schurath, U., Weingartner, E., Gysel, M., and Baltensperger, U.: Coating of soot and $(NH_4)(H_2)SO_4$ particles by ozonolysis products of alpha-pinene, J. Aerosol. Sci., 34, 1297–1321, doi:10.1016/s0021-8502(03)00364-1, 2003.

Title Page

Abstract | Introduction

Conclusions | References

Tables | Figures

⏮ | ⏭

◀ | ▶

Back | Close

Full Screen / Esc

Printer-friendly Version

Interactive Discussion

Spracklen, D. V., Carslaw, K. S., Pöschl, U., Rap, A., and Forster, P. M.: Global cloud condensation nuclei influenced by carbonaceous combustion aerosol, Atmos. Chem. Phys., 11, 9067–9087, doi:10.5194/acp-11-9067-2011, 2011.

Stith, J. L., Twohy, C. H., DeMott, P. J., Baumgardner, D., Campos, T., Gao, R., and Anderson, J.: Observations of ice nuclei and heterogeneous freezing in a Western Pacific extratropical storm, Atmos. Chem. Phys., 11, 6229–6243, doi:10.5194/acp-11-6229-2011, 2011.

Twohy, C. H. and Anderson, J. R.: Droplet nuclei in non-precipitating clouds: composition and size matter, Environ. Res. Lett., 3, 045002, doi:10.1088/1748-9326/3/4/045002, 2008.

Twohy, C. H., Hudson, J. G., Yum, S. S., Anderson, J. R., Durlak, S. K., and Baumgardner, D.: Characteristics of cloud-nucleating aerosols in the Indian Ocean region, J. Geophys. Res.-Atmos., 106, 28699–28710, doi:10.1029/2000jd900779, 2001.

Widmann, J., Yang, J. C., Smith, T. J., Manzello, S. L., and Mulholland, G. W.: Measurement of the optical extinction coefficients of postflame soot in the infrared, Combust. Flame, 134, 119–129, doi:10.1016/s0010-2180(03)00089-0, 2003.

Wyslouzil, B. E., Carleton, K. L., Sonnenfroh, D. M., Rawlins, W. T., and Arnold, S.: Observation of hydration of single, modified carbon aerosols, Geophys. Res. Lett., 21, 2107–2110, doi:10.1029/94gl01588, 1994.

Xie, Z. Q., Blum, J. D., Utsunomiya, S., Ewing, R. C., Wang, X. M., and Sun, L. G.: Summertime carbonaceous aerosols collected in the marine boundary layer of the Arctic Ocean, J. Geophys. Res.-Atmos., 112, doi:10.1029/2006jd007247, 2007.

Yin, J. Y. and Liu, L. H.: Influence of complex component and particle polydispersity on radiative properties of soot aggregate in atmosphere, J. Quant. Spectrosc. Ra., 111, 2115–2126, doi:10.1016/j.jqsrt.2010.05.016, 2010.

Zhang, H. R., Egerton, R. F., and Malac, M.: Local thickness measurement through scattering contrast and electron energy-loss spectroscopy, Micron, 43, 8–15, doi:10.1016/j.micron.2011.07.003, 2012.

Zhang, R. Y., Khalizov, A. F., Pagels, J., Zhang, D., Xue, H. X., and McMurry, P. H.: Variability in morphology, hygroscopicity, and optical properties of soot aerosols during atmospheric processing, P. Natl. Acad. Sci. USA, 105, 10291–10296, doi:10.1073/pnas.0804860105, 2008.

Zhu, J. T., Jia, J. C., Kwong, F. L., and Ng, D. H. L.: Synthesis of bamboo-like carbon nanotubes on a copper foil by catalytic chemical vapor deposition from ethanol, Carbon, 50, 2504–2512, doi:10.1016/j.carbon.2012.01.073, 2012a.

Title Page

Abstract | Introduction

Conclusions | References

Tables | Figures

◀ | ▶

◀ | ▶

Back | Close

Full Screen / Esc

Printer-friendly Version

Interactive Discussion

Zhu, J. T., Jia, J. C., Kwong, F. L., Ng, D. H. L., and Crozier, P. A.: Metal-free synthesis of carbon nanotubes filled with calcium silicate, Carbon, 50, 2666–2669, doi:10.1016/j.carbon.2012.01.071, 2012b.

Zhu, J. T., Jia, J. C., Kwong, F. L., Ng, D. H. L., and Tjong, S. C.: Synthesis of multiwalled carbon nanotubes from bamboo charcoal and the roles of minerals on their growth, Biomass Bioenerg., 36, 12–19, doi:10.1016/j.biombioe.2011.08.023, 2012c.

**Characterization of light-absorbing carbon particles**

J. Zhu et al.

Title Page

Abstract | Introduction

Conclusions | References

Tables | Figures

|◀ | ▶|

◀ | ▶

Back | Close

Full Screen / Esc

Printer-friendly Version

Interactive Discussion

**Table 1.** Parameters for the BSU of soot spherules in three altitudes, Layer No. range, La and $d_{0002}$ are range in number of graphene layers, length and the $d$-spacing of the stacking layers inside BSU, respectively.

| Altitude [m] | | Layer No. range. | La [nm] | $d_{0002}$ [nm] |
|---|---|---|---|---|
| 120 | | 3–6 | 1.04–2.39 | 0.37–0.46 |
| 450 | Spherical | 2–4 | 0.67–1.27 | 0.41–0.53 |
| | Non-spherical | 3–4 | 0.72–1.49 | 0.34–0.45 |
| 1500 | | 3–5 | 0.95–1.63 | 0.40–0.46 |

**Table 2.** Number, volume and their ratio in number, and volume of soot and amorphous carbonaceous spheres on $160\,\mu\text{m}^2$ of the TEM grids at three altitudes.

| Altitude [m] | Collection time [min] | Soot | | Amorphous carbonaceous spheres | | Ratio of amorphous carbonaceous spheres to soot | |
|---|---|---|---|---|---|---|---|
| | | Number | Volume $[10^6\,\text{nm}^3]$ | Number | Volume $[10^8\,\text{nm}^3]$ | Number ratio | Volume ratio |
| 120 | 18 | 294 | 7 | 327 | 18 | 1.1 | 265 |
| 450 | 26 | 79 | 9.5 | 122 | 4.8 | 1.5 | 51 |
| 1500 | 18 | 33 | 0.8 | 339 | 11 | 10.3 | 1400 |

Title Page

Abstract | Introduction

Conclusions | References

Tables | Figures

|◄ | ►|

◄ | ►

Back | Close

Full Screen / Esc

Printer-friendly Version

Interactive Discussion
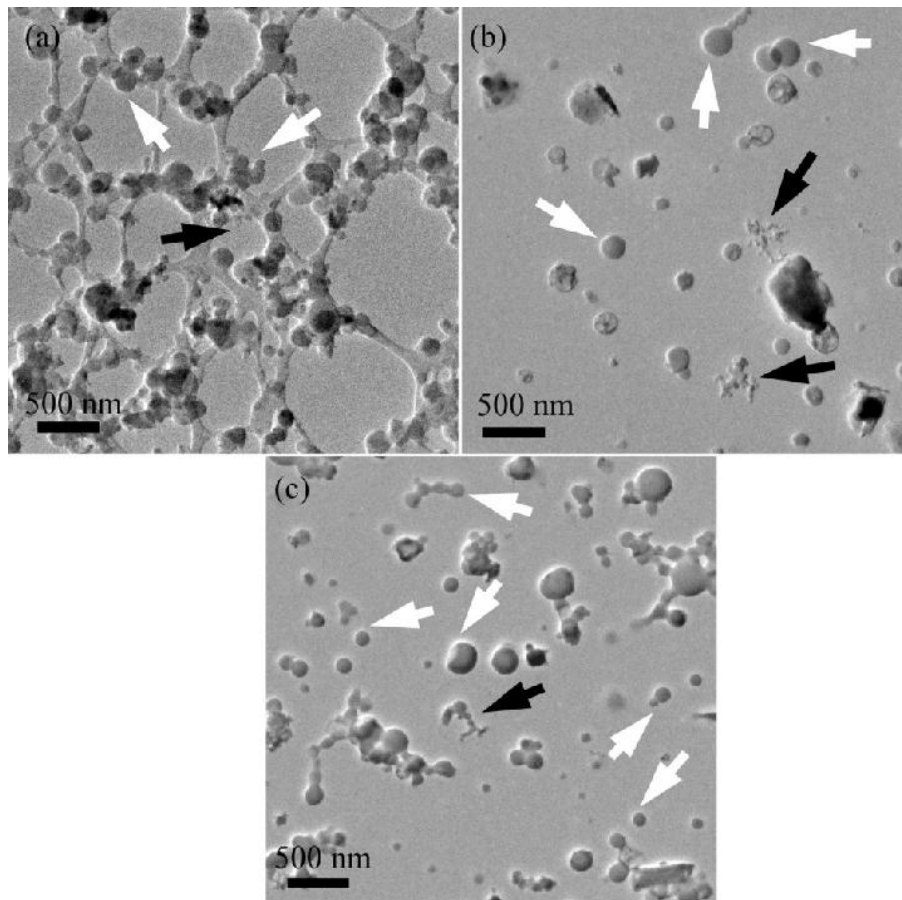
**Fig. 1.** TEM images of aerosols from **(a)** 120, **(b)** 450 and **(c)** 1500 m altitudes. Small spherule soot and brown carbon spheres are marked by black and white arrows, respectively.
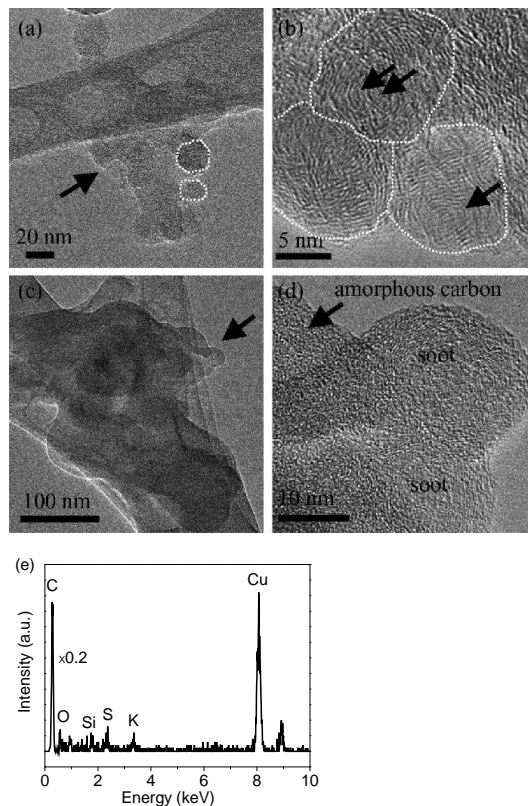
**Fig. 2.** Soot collected at 120 m altitude. **(a)** TEM image of a soot aggregate attached on carbon film and **(b)** HRTEM image from the arrowed area. **(c)** Soot spherules attached on amorphous carbon and **(d)** their HRTEM image from the arrowed area. **(e)** EDS results from the soot in image **(a)**. The intensity of carbon peak is multiplied by factor of 0.2 for comparison with the weak signals from other elements.
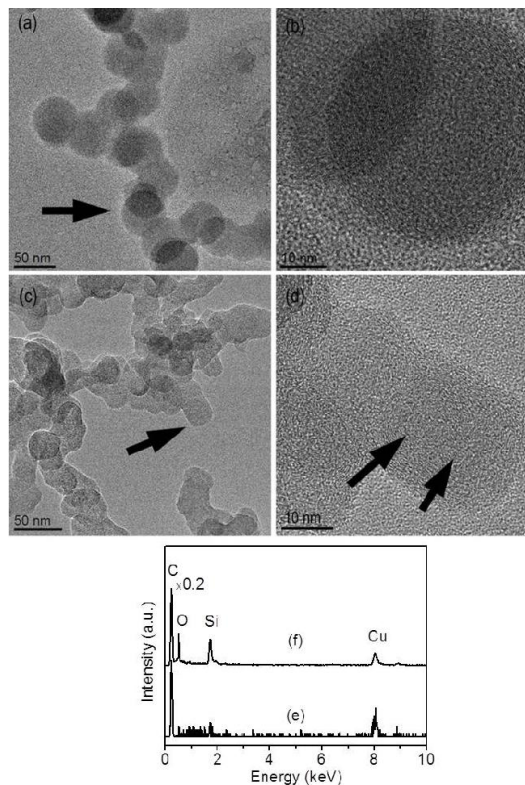
**Fig. 3.** TEM images of, **(a)** soot of spherical subparticles (spherules) and **(b)** their HRTEM image from the arrowed area, **(c)** soot of non-spherical subparticles and **(d)** their HRTEM image from the arrowed area. EDS results **(e, f)** from the soot in image **(a, c)**, respectively. The intensity of the both carbon peaks in **(e)** and **(f)** is multiplied by factor of 0.2 for comparison with the weak signals from other elements.

Title Page

Abstract | Introduction

Conclusions | References

Tables | Figures

◄◄ | ►►

◄ | ►

Back | Close

Full Screen / Esc

Printer-friendly Version

Interactive Discussion
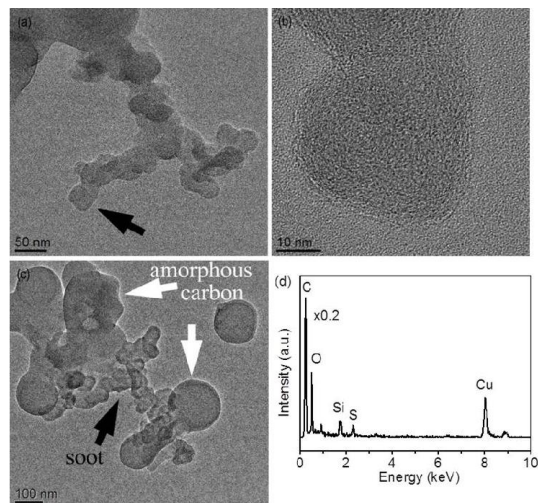
**Fig. 4.** TEM image **(a)** of soot collected at 1500 m and its HRTEM image **(b)** from the arrowed area. **(c)** TEM image of soot (black arrow) mixed with amorphous carbonaceous spheres (white arrows). EDS **(d)** collected from the soot in image **(a)**. The intensity of carbon peak is multiplied by factor of 0.2 for comparison with the weak signals from other elements.
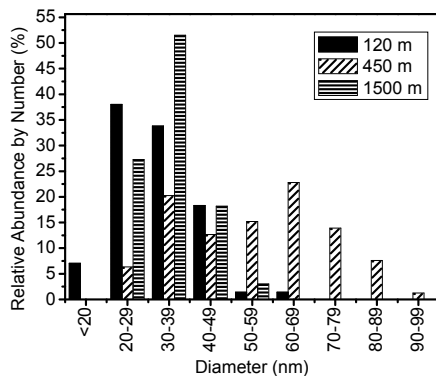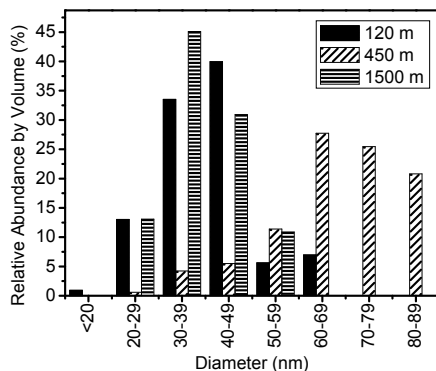
**Fig. 5.** Relative abundance by number **(a)** and volume **(b)** at different diameter for soot primary spherules collected from three altitudes. The average diameters of the soot spherules weighted by number are 30, 55 and 35 nm for 120, 450 and 1500 m, respectively. The average diameters of the soot spherules weighted by volume are 40, 70 and 40 nm for three altitudes.
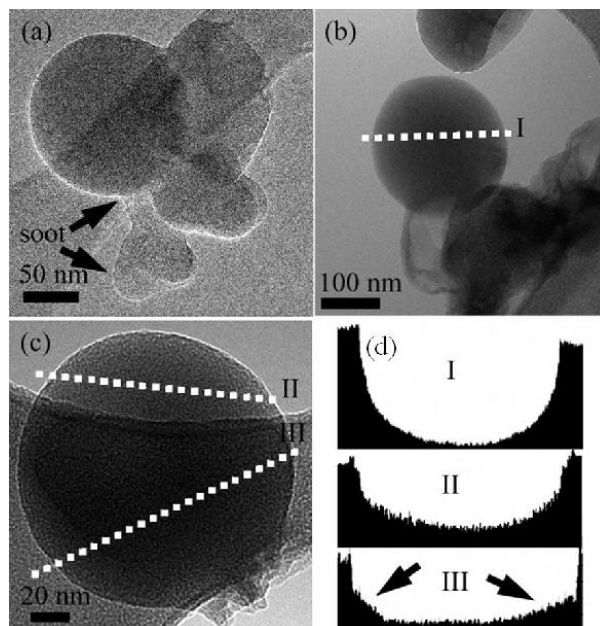
**Fig. 6.** TEM images of amorphous carbonaceous spheres collected at 120 m. **(a)** a sphere mixed with soot particles (arrow), and **(b)** a sphere mixed with possibly organic residue. **(c)** a sphere on the carbon support film. **(d)** Line profiles (I, II, III) come from the dashed lines across the spheres in image **(b)** and **(c)**.

Title Page

Abstract | Introduction

Conclusions | References

Tables | Figures

|◄ | ►|

◄ | ►

Back | Close

Full Screen / Esc

Printer-friendly Version

Interactive Discussion
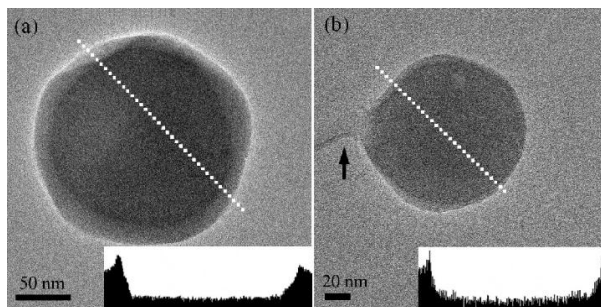


**Fig. 7.** TEM images of **(a)** an amorphous carbonaceous sphere collected at 450 m, **(b)** another one with a tail (arrow). Insets are the profiles for the dashed line across the spheres.
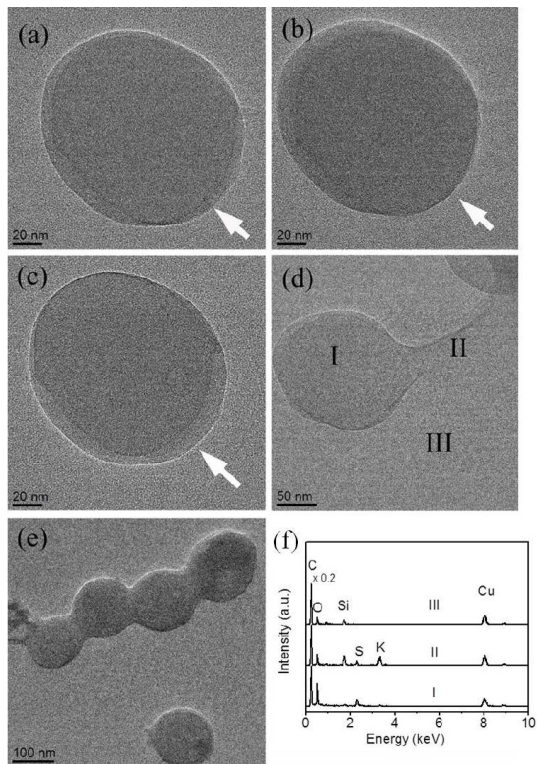
**Fig. 8.** TEM images of: an amorphous carbon sphere (brown carbon) collected at 1500 m, with TEM stage tilted at **(a)** $0^o$, **(b)** $10^o$, **(c)** $-10^o$. **(d)** a brown carbon sphere with a tail. **(e)** four brown carbon spheres connected together in a line. **(f)** EDS from three areas inside image **(d)**. The intensity of carbon peak is multiplied by factor of 0.2 for comparison with the weak signals from other elements.

Discussion Paper | Discussion Paper | Discussion Paper | Discussion Paper |

**ACPD**

12, 32945–32983, 2012

**Characterization of light-absorbing carbon particles**

J. Zhu et al.

Title Page

Abstract | Introduction

Conclusions | References

Tables | Figures

|◄ | ►|

◄ | ►

Back | Close

Full Screen / Esc

Printer-friendly Version

Interactive Discussion

(a)

(b)
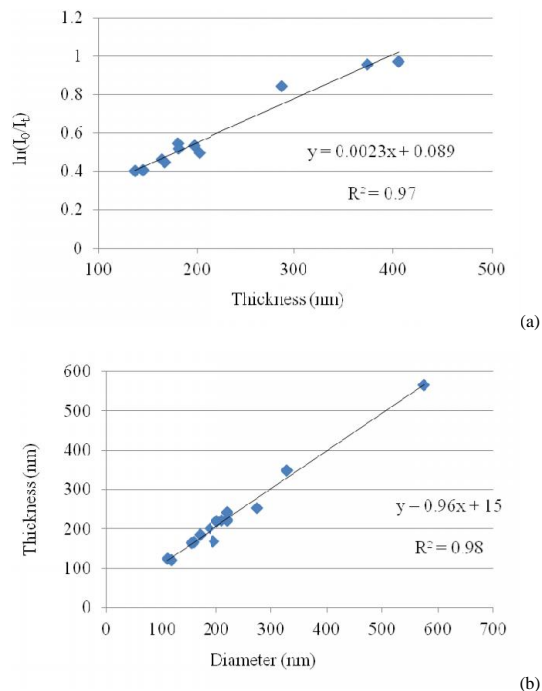
**Fig. 9. (a)** Experimental data of $\ln(I_0 / I_t)$ versus $t$ for absorption coefficient ($\alpha$) from two samples and their linear fitting with equation and square of the correlation coefficient $R^2$. **(b)** The calculated thickness versus measured diameter of amorphous carbonaceous spheres and their linear fitting with equation and square of the correlation coefficient $R^2$. The slope close to 1 indicates their thickness is comparable to their diameter.
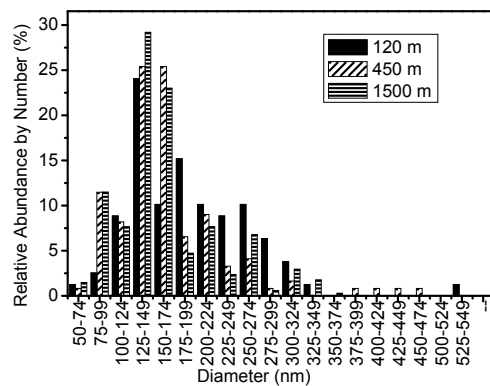
(a)
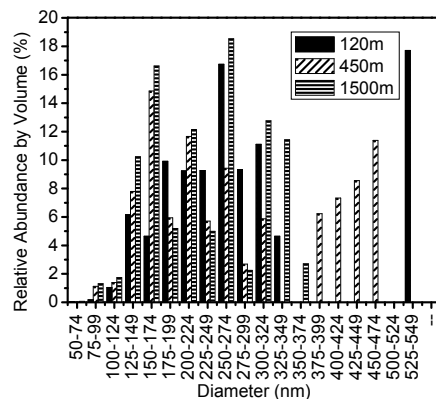
(b)

**Fig. 10.** Relative abundance by number **(a)** and volume **(b)** versus diameter for amorphous carbonaceous spheres collected from three altitudes. The average diameters of the brown carbon spheres weighted by number are 200, 170 and 160 nm for 120, 450 and 1500 m, respectively. The average diameters of the brown carbon spheres weighted by volume are 290, 280 and 235 nm for three altitudes.
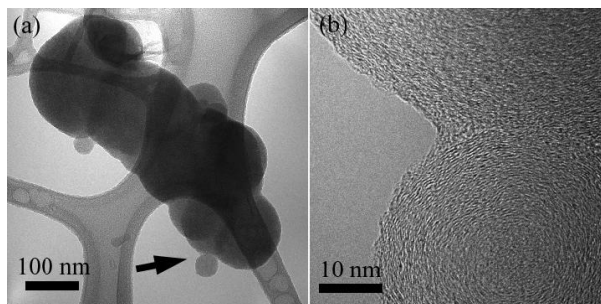
**Fig. 11.** TEM image **(a)** of large spherule soot from 120 m, and HRTEM image **(b)** from the area indicated by arrow.
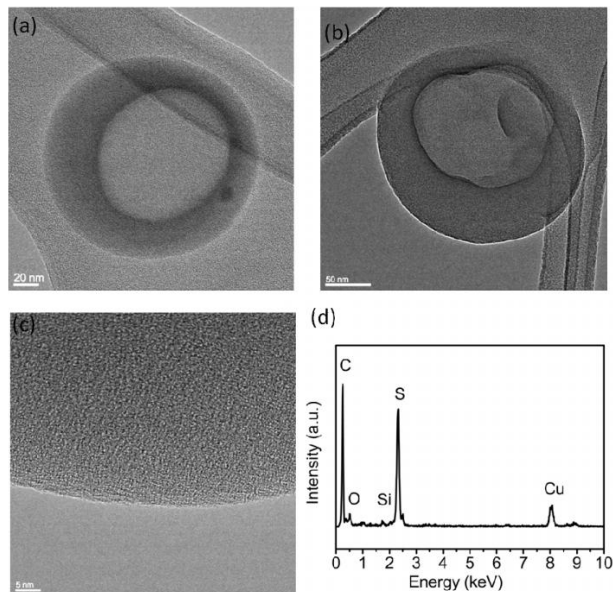
**Fig. 12.** TEM images of cenospheres with different morphologies collected at 120 m (stage 2). **(a)** inner hollow structure, **(b)** another hollow structure, **(c)** the HRTEM image of part of **(b)**. **(d)** EDS collected from the cenosphere in **(b)**.